Supplementary Material

His-Purkinje Network Generation

The His-Purkinje network generation method was based on Gillette et al[1] and is described in detail in the original publication. Figure 1 shows the inputs for the His-Purkinje network generation pipeline (top row). The Purkinje tree is grown on the left ventricle (LV) and on the right ventricle (RV) endocardial surfaces (red surfaces in Figure 1, top row), excluding the base, as this was previously shown to lead to more physiological sinus rhythm activation.[2] Universal ventricular coordinates (UVCs) were defined on the ventricles (Figure 1, top row), consisting of an apico-basal coordinate, ranging continuously from 0 to 1 from apex to base, a transmural coordinate, defined as 0 at the endocardium and 1 at the epicardium, and a rotational coordinate, rotating around the ventricles from $-\pi$ to 0 from the LV free wall to the septum and then back from 0 to $+\pi$ from the septum back to the LV free wall.

The model accounts for three LV fascicles (colors refer to Figure 1, second to fourth row): anterior (purple), septal (orange) and posterior (light-blue), and for two RV fascicles: septal (green) and moderator band (pink). The location of the root points (second row, Figure 1) was provided in terms of UVCs and was based on early activated areas in the Durrer maps. [3] The root points were then used to grow five independent networks that were joined to the His as shown in Figure 1, bottom-right. The His bundle is formed by filaments bundled together and insulated within a common cable.[4] These filaments are predestined to either the left bundle or the right bundle. To represent this anatomical property of the His bundle, we duplicated the His bundle segments in our Purkinje networks. One strand continues into the left bundle and the other continues into the right bundle.

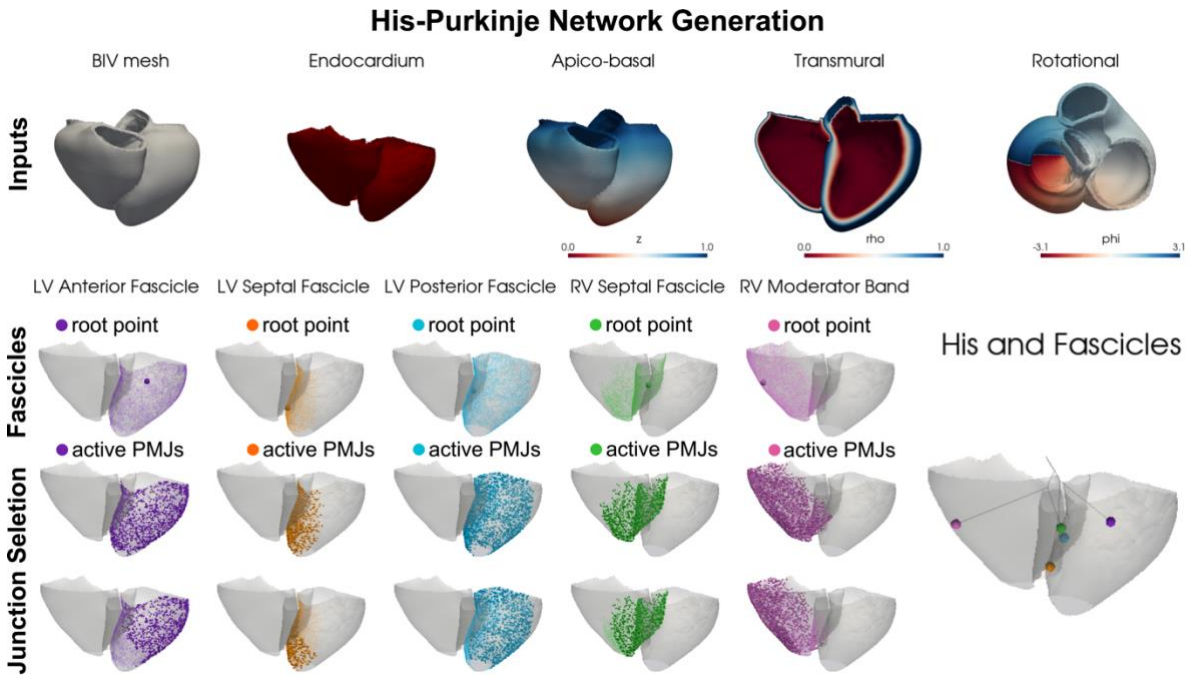

Figure 1 His-Purkinje network generation pipeline. The first row shows the inputs for the His-Purkinje Network generation (from left to right): a biventricular mesh, the left and right ventricular endocardial surfaces the network is grown on, an apico-basal universal ventricular coordinate (UVC), ranging between 0 at the apex and 1 at the base, a transmural UVC, varying from 0 to 1 from the endocardium to the epicardium and a rotational UVC from $-\pi$ to $+\pi$ around the ventricles. The second row shows the root points for the five fascicles included in the modes. The third and rows represent all Purkinje-myocardium junctions (PMJs) and the final PMJs, remaining after deactivating the redundant PMJs. On the right, a picture of the His and fascicles, showing the root points as colored spheres.

The trees associated with the fascicles are grown independently from each other and can therefore overlap. This would not make a difference in sinus rhythm simulations, where the stimulus spreads from the His, fascicles, Purkinje and finally to the myocardium through the Purkinje-myocardium junctions (PMJs), e.g. the terminal points of the His-Purkinje network, as each node can activate only once. On the other hand, during pacing, additional PMJs can affect the simulation as the stimulus can enter the wrong fascicle. To prevent this, we deactivated redundant PMJs. First, the PMJs associated with each fascicle were found (Figure 1, third row). We then identified the portions of LV and RV endocardial surfaces that were covered by each fascicle tree, and we identified areas where the trees overlapped. An eikonal simulation was run on the tree associated with each fascicle by stimulating the root point to find when each terminal point would activate. In areas where the fascicle trees overlapped, only the PMJs with the shortest activation time were connected with the

surrounding myocardium and were therefore activated. The PMJs remaining active after this procedure are shown in Figure 1, bottom row. The image shows that there is no overlap between active PMJs belonging to different fascicles.

The timing of the first activations from the fascicles to ventricular myocardium was based on the Durrer maps. [3] The first LV activation occurs at the three simultaneous fascicle locations (anterior, septal and posterior). Therefore, we computed the conduction velocity (CV) of each LV fascicle separately to guarantee simultaneous activation of the root points of the fascicles. According to the Durrer maps, the RV fascicles activate about 10 ms later than the LV fascicles. Therefore, the CV of the RV fascicles was computed to achieve activation of the RV fascicles root points 10 ms later than the LV.

This network generation pipeline was applied to all twenty-four patient-specific meshes. Proximal LBBB was simulated by disconnecting the left bundle branch from the LV Purkinje network along the His.

Scar mapping

Figure 2 shows the LV lateral wall and septal scar geometries mapped on one of the patient-specific meshes. Black and red regions indicate scar core and border zone, respectively.

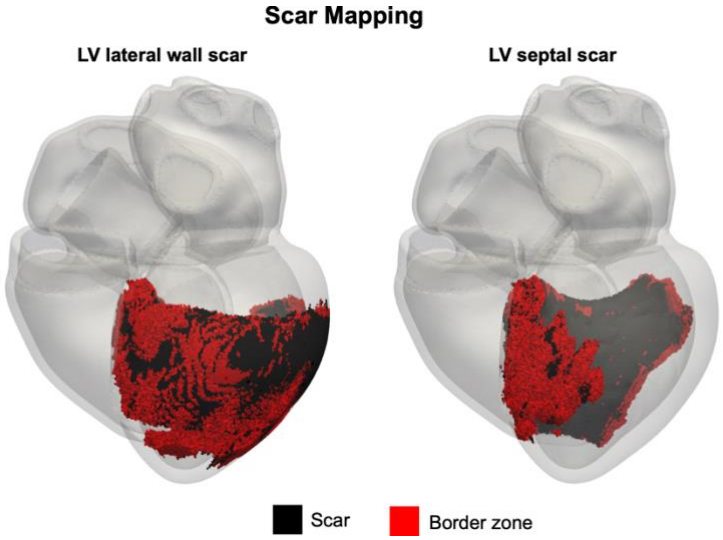

Figure 2 LV lateral wall (left) and septal (right) scar (black) and border zone (red) geometries mapped on one of the patient-specific models.

Model validation

We validated the model using electrocardiographic imaging (ECGi) during baseline left bundle branch block (LBBB) and His bundle pacing (HBP), acquired from 8 LBBB patients as part of two ECGi studies.[5,6] Additionally, simulation results for response to cardiac resynhronization therapy (CRT) and HBP were validated against data published by Arnold et al[7] to verify that the model replicates clinical response to pacing.

Electrocardiographic Imaging data

ECGi data were collected as part of two clinical studies.[5,6] The first study[6] (trial registration number NCT01831518) recruited 11 patients undergoing CRT implantation, including LBBB (N=7) and non-LBBB (N=4) baseline rhythm. For the purpose of this study, we compared our LBBB model against data from 7 LBBB patients. The details about data collection and analysis have been published previously [6]. Briefly, ventricular epicardial activation times were computed from unipolar electrograms as the time of maximum negative slope during the QRS complex. Then, we computed metrics to quantify left ventricular (LV) and biventricular (BIV) activations, similar to what we did for the simulation results: shortest time interval needed to activate 95% of the LV (LVAT95); LV dyssynchronous index (LVDI), computed as the standard deviation of LV activation times; shortest time interval needed to activate 90% of the ventricles (BIVAT90), BIV dyssynchronous index (BIVDI), computed as the standard deviation of ventricular activation times; ventricular electrical uncoupling (VEU) [8], computed as the difference between mean LV activation times and mean right ventricular (RV) activation times. The metrics computed from ECGi data accounted only for the ventricular epicardial surface, while the metrics computed from simulation results accounted for the whole ventricular myocardium. In both cases, the base of the ventricles, including the outflow tracts, was excluded from the mesh. We analyzed 3 baseline beats for each patient, leading to a total of 21 beats.

We considered one additional LBBB patient from a second study[5] (trial registration number NCT 04322877) who also underwent ECGi. 3 baseline LBBB beats were collected and analyzed. This patient also underwent temporary HBP, that led to 2 beats with narrow QRS. We used these two beats to validate the metrics predicted by the model during selective HBP.

LBBB Baseline Validation

Figure 3 shows the comparison between the LBBB baseline metrics measured from the 24 beats extracted from the ECGi data and the metrics predicted by the model for all 24

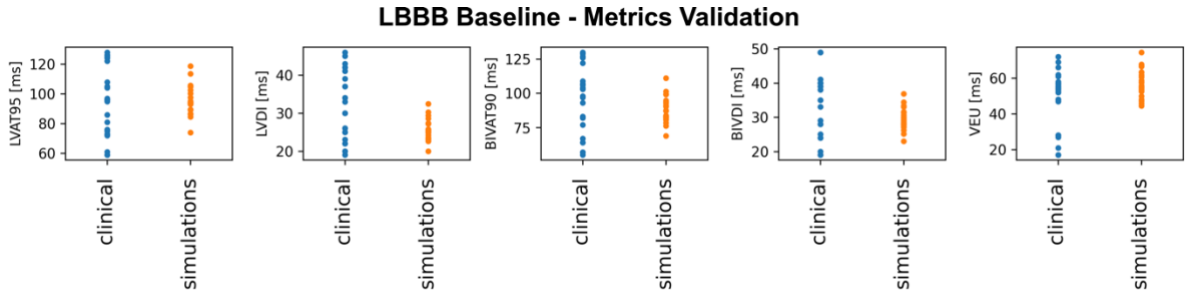

Figure 3 Comparison between ECGi metrics (N=24 beats) from LBBB patients at baseline in blue and metrics predicted by the model (N=24 patients) during LBBB baseline in orange. From left to right: LVAT95, LVDI, BIVAT90, BIVDI and VEU.

patients. All metrics are within physiological ranges, showing that the model can reproduce features of LBBB activation pattern. We also show that the model replicates local LBBB activation by comparing an anterior and a posterior view of the epicardial maps for one

patient at baseline with the epicardial activation times predicted by the model for all patients (Figure 5 and 6).

Pacing Validation

Figure 4 shows a comparison between the metrics extracted from 2 ECGi beats during HBP and the metrics predicted by the model during selective HBP. The model predictions for

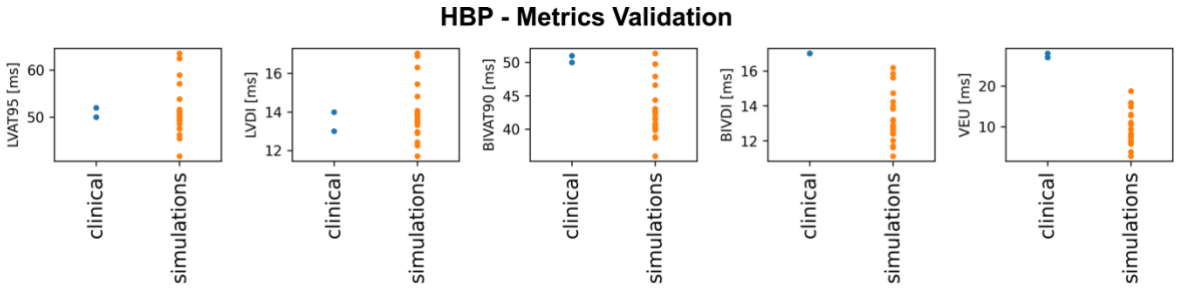

Figure 4 Comparison between ECGi metrics (N=2 beats) from one LBBB patient during HBP in blue and metrics predicted by the model (N=24 patients) during selective HBP in orange. From left to right: LVAT95, LVDI, BIVAT90, BIVDI and VEU.

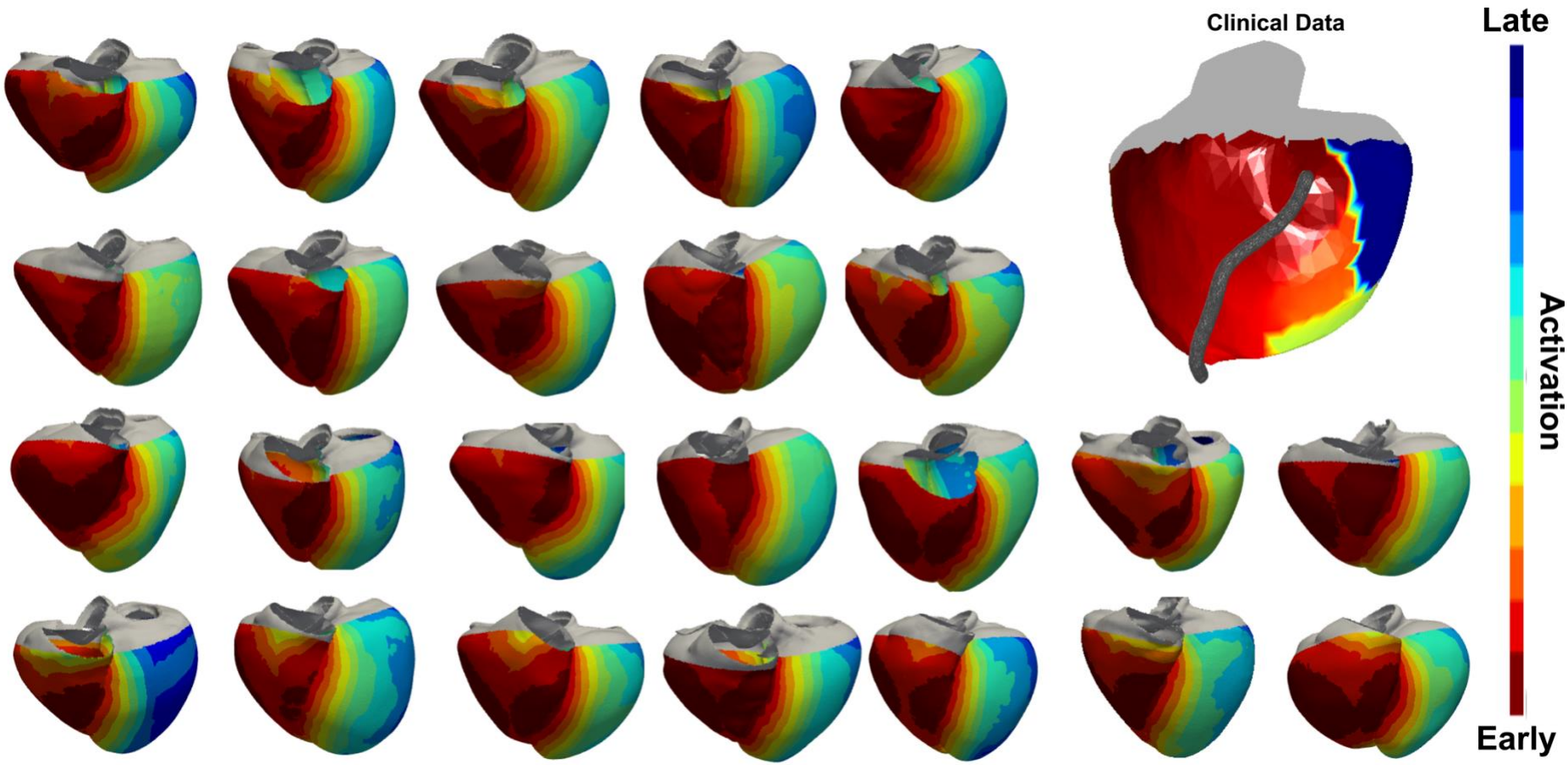

Figure 5 Anterior view of the comparison between epicardial activation measured from ECGi data for one patient (top right) and epicardial activation times predicted by the model for all twenty-four geometries. Red to blue areas show early to late activated regions, while gray areas represent the base of the ventricles, excluded from metrics computation.

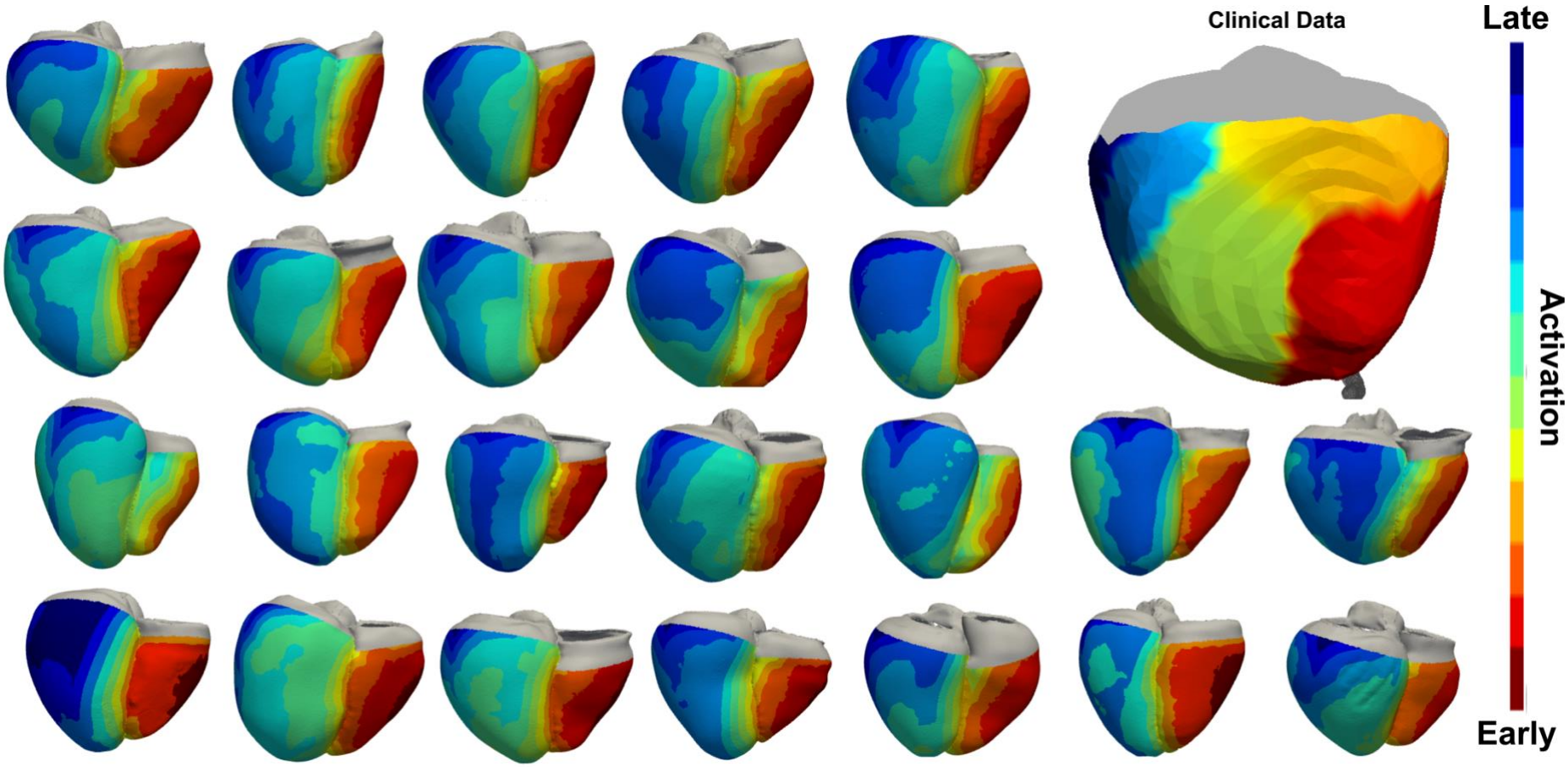

Figure 6 Posterior view of the comparison between epicardial activation measured from ECGi data for one patient (top right) and epicardial activation times predicted by the model for all twenty-four geometries. Red to blue areas show early to late activated regions, while gray areas represent the base of the ventricles, excluded from metrics computation.

LVAT95 and LVDI agree with clinical measurements. However, metrics for biventricular dyssynchrony are underestimated by the model. Nevertheless, we are comparing the model only to two beats, that might not be enough to represent the range of response during HBP.

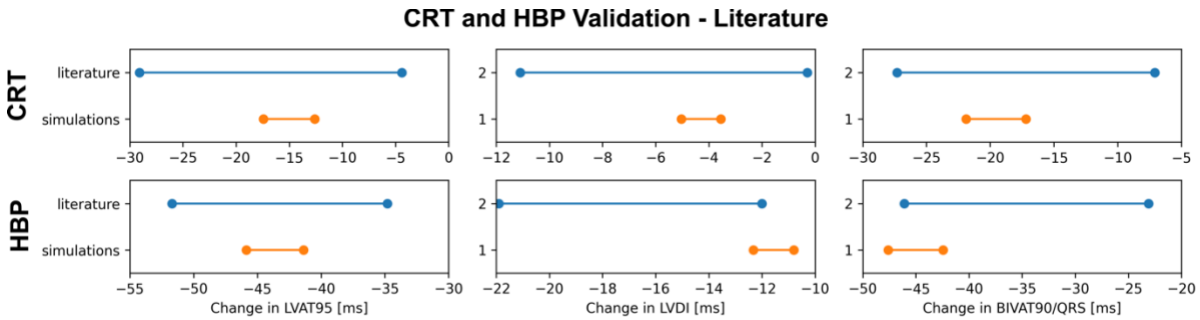

Figure 7 Comparison of response to CRT and HBP predicted by the model (orange) and reported in Arnold et al [7] (blue) in terms of reduction in LVAT95, LVDI and QRS duration, approximated with BIVAT90 in the model. All values are shown as 95% confidence intervals.

To provide a more comprehensive validation of our model during pacing, we also compared model predictions with data published in the literature by Arnold et al [7]. The authors provided 95% confidence intervals (95-CI) for reduction in LVAT95, LVDI and QRS duration induced by standard CRT and HBP from 17 LBBB patients. We compared these values with the 95-CI predicted by the model for reduction in LVAT95, LVDI and BIVAT90, used as a surrogate for QRS duration, induced by CRT (Figure 7, top) and HBP (Figure 7, bottom). The model replicates values for reduction in LVAT95, LVDI and ventricular activation (QRS duration vs BIVAT90) during CRT. Although the values are mostly within reported ranges for HBP as well, the model slightly underestimates response in terms of LVDI and overestimates response to BIVAT90/QRS duration. Nevertheless, we can conclude that the model largely replicates response to different pacing modalities.

The model validation provided in this section shows that the baseline LBBB model reproduces standard LBBB activation patterns with large delays between the RV and the LV activations. We also show that metrics extracted from the model agree with the metrics

computed from ECGi data. Although there are some small differences, the model is also able to predict response to HBP and CRT.

The effect of Purkinje conduction velocity

To investigate the effect of healthy His-Purkinje CV on the conclusion of our study, we repeated all simulations and comparisons with a healthy Purkinje CV of 2 m/s (compared to 3 m/s in the main manuscript). Consistent with the manuscript, we considered the following conduction disturbances: 1) normal His-Purkinje system CV of 2.0 m/s; 2) CV in the LV His-Purkinje system decreased to 1.4 m/s (70% of healthy CV), simulating mild diffuse LV conduction disease; 3) CV in the LV His-Purkinje system reduced to 0.7 m/s (35% of healthy CV), simulating severe diffuse LV conduction disease; 4) CV in ventricular myocardium decreased to 0.42 m/s (70% of healthy CV); 5) CV in ventricular myocardium decreased to 0.21 m/s (35% of healthy CV); 6) large septal non-conducting scar; 7) large non-conducting LV lateral wall scar.

Table 1 summarizes the results of the simulations. Below, we repeat the comparisons performed in the main manuscript.

Slow LV His-Purkinje system and myocardium

Decreasing healthy His-Purkinje CV from 3.0 m/s to 2 m/s did not change the conclusion of the study in the presence of proximal LBBB alone and with slow LV His-Purkinje system or myocardium.

HBP and LBBP remained more effective than standard CRT in the presence of proximal LBBB and otherwise healthy His-Purkinje system in terms of both LV (LVAT-95: CRT 90.8±8.9 ms vs HBP 60.3±5.6 ms, $P<0.01$ vs LBBP 70.0±7.5 ms, $P<0.01$) and BIV (BIVAT-90: CRT 77.2±8.3 ms vs HBP 49.5±4.3 ms, $P<0.01$ vs LBBP 56.6±6.3 ms, $P<0.01$) activation times. A moderate decrease in LV His-Purkinje CV from 2.0 m/s to 1.4 m/s also

led to better response with HBP and LBBP compared to standard CRT (P<0.01 for all metrics). CRT was significantly better than HBP and LBBP in the presence of severe CV slowing of the LV His-Purkinje system (from 2.0 m/s to 0.7 m/s) in terms of all metrics (Table 1).

Consistent with the manuscript, HOT-CRT and LOT-CRT improved response compared to HBP and LBBP in the presence of severely slow LV His-Purkinje system (P<0.01 for all metrics, Table 1). However, LV and BIV activation times were comparable between CRT and HOT-CRT, while LOT-CRT was better than CRT alone. This differs from the results presented in the main manuscript, where LV activation times were shorter with HOT-CRT compared to CRT alone, indicating that slower His-Purkinje conduction is unfavorable to CSP.

The considerations reported in the main manuscript in the presence of slower myocardial CV did not change when healthy His-Purkinje CV was decreased from 3 m/s to 2 m/s. Moderate and severe ventricular myocardium conduction slowing but normal His-Purkinje CV led to better response with HBP and LBBP compared to CRT (P<0.01 for all metrics, Table 1). HOT-CRT and LOT-CRT were comparable to HBP and LBBP alone, respectively, in terms of both BIV and LV activation times.

Septal and LV lateral wall scar

The conclusions presented in the manuscript in the presence of septal scar did not change when the healthy His-Purkinje CV was decreased from 3 m/s to 2 m/s. HBP and LBBP were still ineffective in the presence of non-conductive septal scar, leading to LV and BIV activation times comparable to baseline (Table 1). On the other hand, CRT remained effective at shortening both LV and BIV activation times compared to baseline, with differences being statistically significant for all metrics. LVAT-95 were comparable between

CRT, HBP and LBBP (Table 1), while BIVAT-90 were better with CRT compared to HOT-CRT and LOT-CRT, although the differences were not statistically significant (P=0.17 CRT vs HOT-CRT, P=0.11 CRT vs LOT-CRT).

Changing the healthy His-Purkinje CV from 3 m/s to 2 m/s led to differences in response to pacing in the presence of LV lateral wall scar. While CRT was ineffective in shortening LV activation times when the Purkinje CV was 3 m/s, LVAT-95 (baseline: 164.1±15.5 ms vs CRT: 114.0±13.4 ms, P<0.01) and BIVAT-90 (baseline: 140.8±13.4 ms vs CRT: 142.7±19.2 ms, P<0.01) were shortened by CRT compared to baseline when the Purkinje CV was 2 m/s. Furthermore, reductions in LVAT-95 and BIVAT-90 achieved with CRT were comparable to those achieved during HBP (LVAT-95: 115.2±12.9 ms, P=0.9 vs CRT; BIVAT-90: 115.2±12.9 ms, P=0.9 vs CRT) and LBBP (LVAT-95: 114.0±12.7 ms, P=0.84 vs CRT; BIVAT-90: 114.0±12.7 ms, P=0.9 vs CRT). Finally, HOT-CRT and LOT-CRT led to improved LVAT-95 and BIVAT-90 compared to CRT, HBP and LBP alone when the CV of healthy His-Purkinje system was set to 2 m/s (Table 1). These changes are caused by the fact that baseline, HBP and LBBP activation times in the presence of LV lateral wall are increased by the slower His-Purkinje CV (Purkinje CV 3 m/s vs 2 m/s: baseline 148.0±15.2 ms vs 164.1±15.5 ms; HBP 129.2±14.1 ms vs 140.1±14.7 ms; LBBP 125.4±14.0 ms vs 137.4±14.1 ms). On the other hand, activation times simulated during CRT were largely unaltered by a change in the His-Purkinje CV (Purkinje CV 3 m/s vs 2 m/s: 142.2±19.6 ms vs 142.7±19.2 ms) because the activation wave does not enter the distal His-Purkinje system due to the scar.

Changing healthy His-Purkinje CV from 3 m/s to 2 m/s did not affect the conclusions of the study in the presence of proximal LBBB alone and combined with slow LV His-Purkinje system, slow myocardium and non-conductive septal scar. However, the results changed in the presence of proximal LBBB and non-conductive LV lateral wall scar.

Table 1 Results summary. Simulated BIVAT-90 (top section) and LVAT-95 (bottom section) during baseline, CRT, selective HBP (S-HBP) and LBBP (S-LBBP), HOT-CRT and LOT-CRT for different conduction disturbances with a healthy Purkinje CV of 2 m/s.

Biventricular response – BIVAT-90						
	Baseline	**CRT**	**S-HBP**	**S-LBBP**	**HOT-CRT**	**LOT-CRT**
LBBB	101.7 ± 9.6	77.2 ± 8.3	49.5 ± 4.3	56.6 ± 6.3	-	-
LBBB & moderately slow LV Purkinje	117.4 ± 10.5	87.4 ± 9.0	62.3 ± 5.5	69.8 ± 8.0	56.4 ± 4.9	61.3 ± 6.3
LBBB & severely slow LV Purkinje	157.8 ± 13.6	96.4 ± 9.1	134.4 ± 10.1	117.2 ± 13.0	100.1 ± 8.1	83.1 ± 8.5
LBBB & moderately slow myocardium	121.2 ± 13.2	92.9 ± 11.6	61.1 ± 5.5	67.6 ± 7.2	57.5 ± 4.9	63.0 ± 6.0
LBBB & severely slow myocardium	186.6 ± 26.1	144.2 ± 24.1	102.5 ± 10.1	108.1 ± 11.1	99.3 ± 9.5	103.7 ± 10.1
LBBB & septal scar	133.5 ± 12.0	93.6 ± 10.3	131.5 ± 16.1	132.4 ± 14.0	102.5 ± 11.9	103.3 ± 11.0
LBBB & LV lateral wall scar	140.8 ± 13.4	114.0 ± 13.4	115.2 ± 12.9	114.0 ± 12.7	99.9 ± 14.5	99.1 ± 14.5
Left ventricular response – LVAT-95						
LBBB	110.2 ± 9.9	90.8 ± 8.9	60.3 ± 5.6	70.0 ± 7.5	-	-
LBBB & moderately slow LV Purkinje	128.0 ± 10.8	102.6 ± 9.6	74.4 ± 6.5	86.5 ± 8.8	64.4 ± 5.4	74.7 ± 7.0
LBBB & severely slow LV Purkinje	174.7 ± 12.7	111.0 ± 10.2	149.7 ± 11.2	140.8 ± 13.0	112.4 ± 9.8	100.5 ± 10.1
LBBB & moderately slow myocardium	131.5 ± 13.6	108.3 ± 11.0	74.2 ± 7.0	83.6 ± 9.0	67.5 ± 5.4	75.8 ± 7.2
LBBB & severely slow myocardium	204.3 ± 26.5	164.4 ± 22.0	122.9 ± 12.1	131.4 ± 14.0	115.2 ± 9.9	122.5 ± 11.4
LBBB & septal scar	145.2 ± 12.2	110.1 ± 10.8	143.7 ± 14.8	144.5 ± 12.8	110.4 ± 11.4	110.8 ± 11.1
LBBB & LV lateral wall scar	164.1 ± 15.5	142.7 ± 19.2	140.1 ± 14.7	137.4 ± 14.1	127.8 ± 14.7	126.8 ± 14.5

The effect of His-Purkinje system viability in the presence of septal scar

What happens to the LV His-Purkinje system in the presence of septal scar is unknown. To investigate the effect of how the LV His-Purkinje conduction properties change within the scar, we performed additional simulations with the following scenarios: 1) non-conductive septal scar and non-conductive His-Purkinje system within the scar (consistent with the results in the main manuscript); 2) non-conductive septal scar and conductive His-Purkinje system within the scar with a healthy CV of 3 m/s; 3) non-conductive septal scar and conductive His-Purkinje system within the scar with moderately slow CV of 2.1 m/s (70% of healthy CV); 4) non-conductive septal scar and conductive His-Purkinje system within the scar with severely slow CV of 1.05 m/s (35% of healthy CV). We then computed response metrics during LBBB baseline, CRT, HBP, LBBP, HOT-CRT and LOT-CRT as reported in the main manuscript.

Figure 8 Effect of LV His-Purkinje conduction within septal scar. Bar chart of LVAT-95, LVDI, BIVAT-90 and BIVDI for non-conductive septal scar and non-conductive septal Purkinje (blue), conductive healthy septal Purkinje (orange), moderately slow conductive septal Purkinje (green) and severely slow conductive septal Purkinje (purple). The values are presented as mean ± standard deviation (black lines). LVAT-95 = 95% LV activation time, LVDI = LV dyssynchronous index, BIVAT-90 = 90% biventricular activation time, BIVDI = biventricular dyssynchronous index, LBBB = left bundle branch block, CRT = cardiac resynchronization therapy, S-HBP = selective His bundle pacing, S-LBBP optAVD = selective left bundle pacing with optimized atrioventricular delay, HOT-CRT = His optimized CRT, LOT-CRT = left bundle optimized CRT

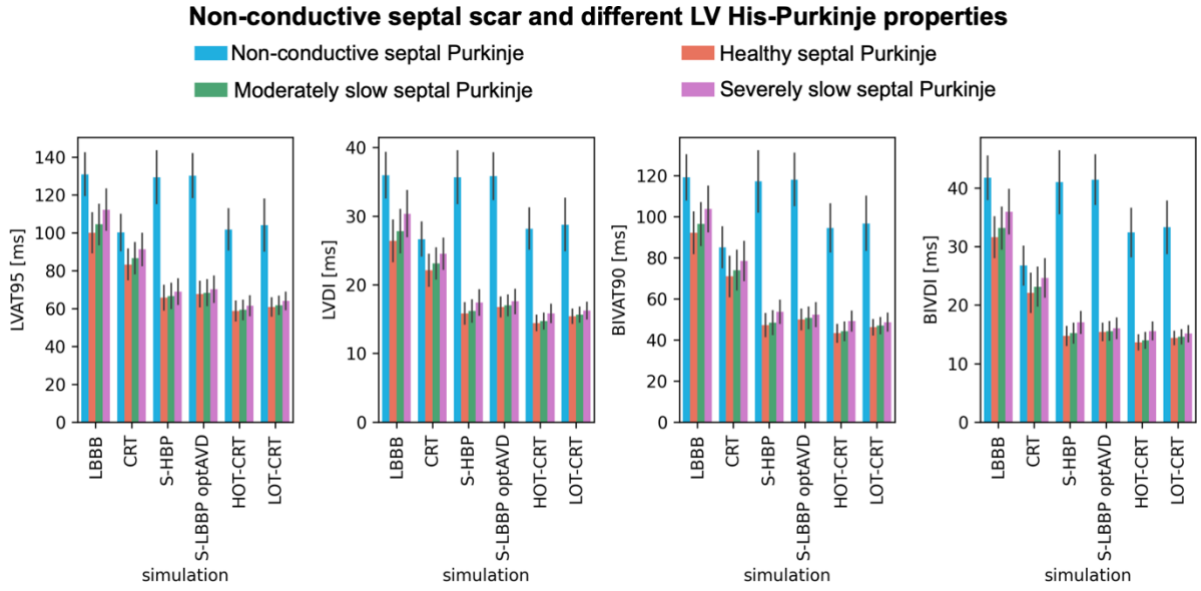

The results are presented in Figure 8 and in Table 2. In the presence of proximal LBBB, non-conductive septal scar but viable healthy His-Purkinje within the scar, HBP and LBBP were more effective than CRT. LVAT-95 with HBP and LBBP were 65.7±6.5 and 67.6±6.6 ms, respectively, and were significantly shorter than baseline (100.0±10.5 ms, P<0.01) and CRT (83.2±8.0 ms). Similarly, BIVAT-90 were significantly better with HBP (47.2±5.6 ms) and LBP (50.0±4.9 ms) compared to CRT (70.9±9.6 ms, P<0.01). However, HOT-CRT and LOT-CRT did not bring additional benefits in ventricular activation times compared to HBP (HBP: 47.2±5.6 ms, HOT-CRT: 43.2±4.2 ms, P=0.36) and LBBP alone (LBBP: 50.0±4.9 ms, LOT-CRT: 46.2±3.7 ms, P=0.40), respectively.

These considerations did not change when the His-Purkinje system within the septal scar was conductive but moderately or severely slow. HBP and LBBP were still more effective than CRT in both cases (see Table 2 and Figure 8, green and purple), with significant statistical differences for all metrics (P<0.01). HOT-CRT and LOT-CRT did not lead to significant improvements in ventricular activation times compared to HBP and LBBP alone. When the His-Purkinje system within the septal was severely slow, BIVAT-90 were 53.7±5.5 ms and 49.2±4.6 ms with HBP and HOT-CRT (P=0.27), and 52.4±5.7 ms and 48.7±4.3 ms (P=0.52) with LBBP and LOT-CRT, respectively.

These results indicate that, if the Purkinje within the septal scar is viable, even if slow, HBP and LBBP do not lose their efficacy in resynchronizing the electrical activation of the ventricles. On the other hand, if the Purkinje with the septal scar is also non-conductive, then conduction system pacing is ineffective and CRT represents a better alternative, as shown in the manuscript.

Table 2 Results summary. Simulated BIVAT-90 (top section) and LVAT-95 (bottom section) during baseline, CRT, selective HBP (S-HBP) and LBBP (S-LBBP), HOT-CRT and LOT-CRT for different scenarios with septal scar.

Biventricular response – BIVAT-90						
	Baseline	**CRT**	**S-HBP**	**S-LBBP**	**HOT-CRT**	**LOT-CRT**
LBBB, septal scar & non-viable septal Purkinje	119.1 ± 10.8	85.1 ± 9.8	117.2 ± 14.9	118.1 ± 12.9	94.5 ± 11.6	96.7 ± 13.0
LBBB, septal scar & healthy septal Purkinje	92.2 ± 10.0	70.9 ± 9.6	47.2 ± 5.6	50.0 ± 4.9	43.2 ± 4.2	46.2 ± 3.7
LBBB, septal scar & viable moderately slow septal Purkinje	96.4 ± 10.3	74.0 ± 9.6	48.3 ± 5.7	50.8 ± 5.1	44.2 ± 4.3	47.0 ± 3.8
LBBB, septal scar & viable severely slow septal Purkinje	103.8 ± 11.0	78.4 ± 9.4	53.7 ± 5.5	52.4 ± 5.7	49.2 ± 4.6	48.7 ± 4.3
Left ventricular response – LVAT-95						
LBBB, septal scar & non-viable septal Purkinje	130.9 ± 11.2	100.1 ± 9.5	129.4 ± 13.9	130.2 ± 11.6	101.7 ± 10.7	104.1 ± 13.6
LBBB, septal scar & healthy septal Purkinje	100.0 ± 10.5	83.2 ± 8.0	65.7 ± 6.5	67.6 ± 6.6	58.7 ± 5.1	60.8 ± 4.7
LBBB, septal scar & viable moderately slow septal Purkinje	104.4 ± 10.5	86.5 ± 8.1	66.6 ± 6.5	68.3 ± 6.7	59.3 ± 5.0	61.7 ± 4.6
LBBB, septal scar & viable severely slow septal Purkinje	112.2 ± 10.7	91.2 ± 8.5	68.9 ± 6.6	70.2 ± 6.8	61.5 ± 5.1	64.1 ± 4.5

References

1. Gillette K, Gsell MAF, Bouyssier J, et al. Automated Framework for the Inclusion of a His–Purkinje System in Cardiac Digital Twins of Ventricular Electrophysiology. *Annals of Biomedical Engineering*. 2021;49(12). doi:10.1007/s10439-021-02825-9
2. Strocchi M, Lee AWC, Neic A, et al. His-bundle and left bundle pacing with optimized atrioventricular delay achieve superior electrical synchrony over endocardial and epicardial pacing in left bundle branch block patients. *Heart Rhythm*. 2020;17(11). doi:10.1016/j.hrthm.2020.06.028
3. Durrer D, van Dam RT, Freud GE, Janse MJ, Meijler FL, Arzbaecher RC. Total excitation of the isolated human heart. *Circulation*. 1970;41(6). doi:10.1161/01.CIR.41.6.899
4. Vijayaraman P, Chung MK, Dandamudi G, et al. His Bundle Pacing. *J Am Coll Cardiol*. 2018;72(8):927-947. doi:10.1016/j.jacc.2018.06.017
5. Elliott MK, Mehta V, Sidhu BS, Niederer S, Rinaldi CA. Electrocardiographic imaging of His bundle, left bundle branch, epicardial, and endocardial left ventricular pacing to achieve cardiac resynchronization therapy. *HeartRhythm Case Reports*. 2020;6(7). doi:10.1016/j.hrcr.2020.04.012
6. Elliott MK, Strocchi M, Mehta VS, et al. Dispersion of repolarization increases with cardiac resynchronization therapy and is associated with left ventricular reverse remodeling. *Journal of Electrocardiology*. Published online 2022.
7. Arnold AD, Shun-Shin MJ, Keene D, et al. His resynchronization therapy vs. biventricular pacing for heart failure with LBBB: a within-patient comparison of effects on acute haemodynamic function and ventricular activation. *Europace*. 2018;20.

8. Ploux S, Eschalier R, Whinnett ZI, et al. Electrical dyssynchrony induced by biventricular pacing: Implications for patient selection and therapy improvement. *Heart Rhythm*. 2015;12(4). doi:10.1016/j.hrthm.2014.12.031